Improvement of Isolation and Bandwidth of Notch Ultra-Wideband MIMO Antenna on Metamaterial Wall

Shuming Liu, Jingchang Nan*, and Yifei Wang

College of Telecommunications, Liaoning Technical University, Huludao, TX 125000, China

ABSTRACT: This paper presents a novel notch-based ultra-wideband (UWB) MIMO antenna with a metamaterial wall (MLB-MW) designed to significantly enhance the isolation and operational bandwidth between antenna elements. The antenna adopts a 2×1 notch UWB structure, integrating a metamaterial wall made of metallic lines, with an overall size of $20 \times 40 \times 1.6 \, \text{mm}^3$, and utilizes an FR-4 dielectric substrate ($\epsilon_r = 4.4$, $\tan \delta = 0.02$). By leveraging the μ-negative characteristics of the MLB-MW, the antenna achieves a 10 dB improvement in isolation across the C, X, and Ku frequency bands. Its impedance bandwidth ($|S_{11}| < 10 \, \text{dB}$) extends from 6.09–13.07 GHz to 5.51–15 GHz, with a relative expansion rate of 36%. Additionally, key performance parameters of the MIMO antenna are comprehensively evaluated: the envelope correlation coefficient (ECC) remains below 0.01 across the entire frequency band; the diversity gain (DG) is close to 10 dB; and the total active reflection coefficient (TARC) stays below $-10 \, \text{dB}$ across the entire operating band, indicating excellent channel independence and diversity performance. Experimental results verify the feasibility and effectiveness of this antenna in 5G base station applications.

1. INTRODUCTION

Wireless antennas play a crucial role in communication due to their ability to radiate and receive radio waves. With the rapid development of radio technology, a single antenna is becoming increasingly insufficient to meet the demands. Multiple-input multiple-output (MIMO) antennas can simultaneously transmit and receive multiple data streams within one channel, significantly improving the antenna's transmission rate and reliability without increasing spectrum resources [1–4]. However, in a MIMO antenna system, when one antenna is excited, other antennas will induce currents, leading to a degradation in the isolation of the excited antenna and distortion of the radiation pattern, a phenomenon known as coupling. When antenna elements are too far apart, it leads to an increase in antenna size, which is unfavorable for the miniaturization design of mobile devices [5–7]. Therefore, improving the isolation between MIMO antenna elements has become an important area of research for many scholars [8]. Current decoupling methods mainly include neutralization line decoupling, defective ground structure decoupling, decoupling circuit decoupling, and parasitic structure decoupling [9–11].

Ultra-wideband (UWB) antennas are known for their low power consumption and high transmission speeds. Within the bandwidth range of UWB antennas, there are many narrowband frequency bands, such as WiMAX (3.3–3.6 GHz) band, WLAN (5.15–5.85 GHz) band, and X-band uplink (7.9–8.4 GHz) band [12–15]. These narrowband frequency bands can interfere with the performance of the antenna. To solve this problem, scholars have introduced notch techniques [16]. The technical approaches for achieving UWB characteristics

and notch functions are diverse. In terms of bandwidth extension, mainstream methods include: polygonal radiation patch technology (such as circular or elliptical patches), which broadens the bandwidth by exciting multiple resonant modes. While simple in structure, its ability to extend bandwidth is limited; parasitic units and coupled feeding techniques, which introduce additional resonant points to effectively widen the bandwidth. They are flexible in design but usually increase the antenna size and complexity; and fractal structure technology, which utilizes self-similarity to elongate current paths for miniaturization and bandwidth extension. However, its design and optimization processes are complicated [16–18]. In contrast, slotting technology, which involves etching specific slits such as U-shaped or E-shaped slots on the radiation patch or ground plane, significantly disturbs the surface current distribution, exciting multiple closely spaced resonant modes that ultimately merge into an extremely wide impedance bandwidth. This method is flexible in design, effective, and almost does not increase the antenna's physical size or manufacturing cost, offering an attractive solution for the realization of high-performance, miniaturized UWB antennas. In this paper, slotting method is used to achieve UWB characteristics and notch functions of the antenna.

In recent years, metamaterials, due to their extraordinary electromagnetic properties (such as negative refractive index and negative permeability), have provided a new dimension for antenna design. In MIMO system decoupling applications, metamaterial structures have shown great potential. For example, Sun et al. [2] effectively enhanced isolation using a defect ground structure, but the bandwidth was limited. Kong et al. [3] and Nie et al. [5] achieved good performance in compact spaces through shared structures or modal analysis, but their

---

* Corresponding author: Jingchang Nan (nanjingchang@lntu.edu.cn).

designs typically optimize a single metric (isolation or bandwidth). More cutting-edge work includes the exploration by Dutta et al. [4] and Yang et al. [12] of ultra-wideband artificial magnetic conductors (AMCs) in millimeter-wave MIMO antennas, demonstrating the potential of metamaterials in broadband decoupling. However, most of these works focus on using the bandgap or reflective phase properties of metamaterials to suppress surface waves and improve isolation, with little exploration into using their resonant characteristics to simultaneously extend the working bandwidth of the antenna.

This paper presents a notch ultra-wideband (UWB) antenna based on a metal-line metamaterial wall (MLB-MW), which achieves UWB characteristics through the structure of floor corner cutting, slotting, and stepped patch design. By incorporating MLB-MW, the proposed antenna simultaneously improves both isolation and bandwidth for a notch ultra-wideband MIMO antenna. Compared to existing UWB MIMO antennas, the main contributions of this antenna are as follows:

(1) A new method is proposed that uses MLB-MW to simultaneously improve isolation and bandwidth. The isolation improvement is achieved through the mu-negative (MNG) metamaterial characteristics of MLB-MW, and the bandwidth enhancement is obtained through additional resonance.

(2) The maximum isolation is improved by 10 dB. Meanwhile, the impedance bandwidth is increased by 36%. The proposed MIMO antenna operates in the C, X, Ku frequency bands, with a center-to-center distance of 13.6 mm and a height of 1.6 mm, making it suitable for 5G base station applications.

2. DESIGN AND MECHANISMS

The overall structure of the proposed MIMO antenna is shown in Figure 1. Two notch ultra-wideband antennas are printed on a standard substrate. The MLB-MW is placed vertically at the center of the substrate, consisting of 1×2 MNG units printed on
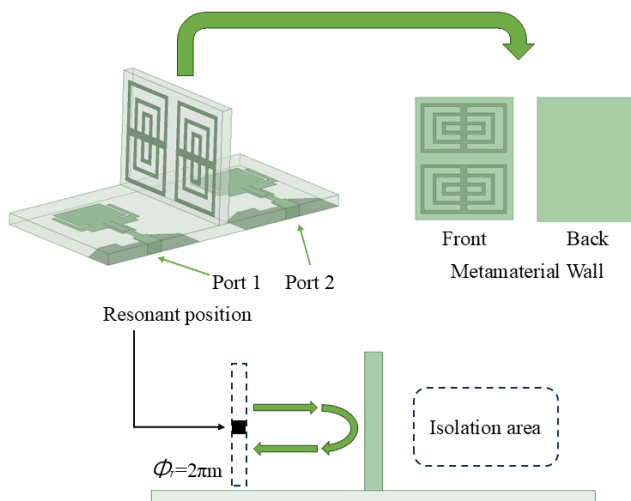

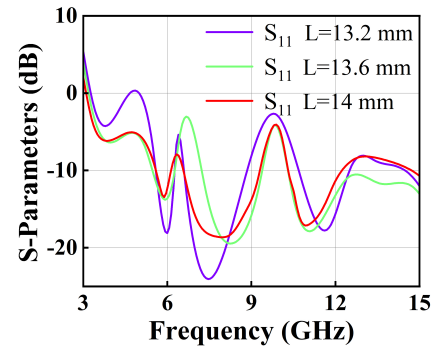**FIGURE 1.** Overall structure of the proposed MIMO antenna.

FIGURE 2. The S_{11} corresponding to different antenna spacings.

one side of the vertical substrate. As shown in Figure 2, the S_{11} performance is optimal when the antenna spacing is 13.6 mm; therefore, the antenna spacing is set to 13.6 mm. In this design, the antenna elements are arranged in a parallel configuration, with an optimized center spacing of 13.6 mm (approximately 0.36λ at 8 GHz). This decision is based on a comprehensive trade-off of performance, compactness, and technical validation. This specific spacing strikes a balance between strong mutual coupling and excessive size, providing an ideal foundation for the subsequent enhancement of decoupling through metamaterial walls. The choice of a parallel layout, as opposed to an orthogonal one, ensures consistency in the radiation pattern to achieve a stable low envelope correlation coefficient. Additionally, this layout is more conducive to system integration and, under the configuration with the strongest electromagnetic coupling, allows for the most effective validation of the proposed metamaterial wall decoupling technique.

When electromagnetic waves strike a nearly lossless normal material, the refractive index (n) can be calculated from the material's structural parameters using the following formula [19]:

$$n = \pm\sqrt{\mu\epsilon} \qquad (1)$$

The refractive index of MNG can be expressed as: $n = \sqrt{(+1)|\epsilon|(-1)\mu|} = i\sqrt{|\epsilon||\mu|}$. Since n is purely imaginary, MNG can prohibit the propagation of electromagnetic waves. Due to the resonance of MNG with electromagnetic waves, it behaves like a large Perfect Electric Conductor (PEC). The MNG isolation wall effectively reduces the coupling energy between antennas.
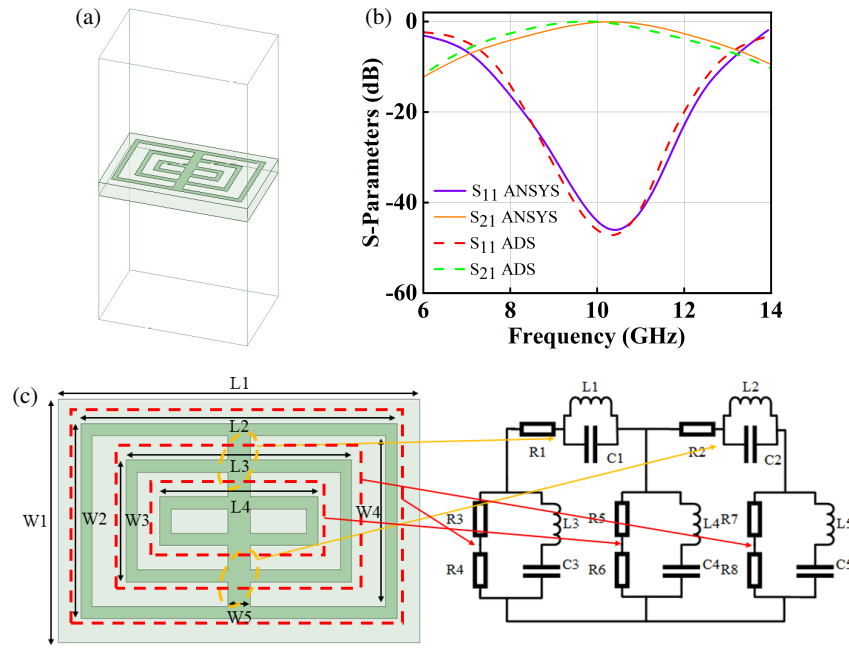
The reflectivity (r) of MNG can be derived from n using the Fresnel formula and Snell's law:

$$r = \frac{\cos(\theta_1) - \sqrt{n^2 - \sin^2(\theta_1)}}{\cos(\theta_1) + \sqrt{n^2 - \sin^2(\theta_1)}} \qquad (2)$$

where θ_1 is the angle of incidence. Apparently, $\sqrt{n^2 - \sin^2(\theta_1)}$ is a pure imaginary number as $n^2 < 0$. Therefore, Equation (2) can be rewritten as:

$$r = 1 + i \cdot \frac{2\cos\theta_1\sqrt{\sin^2(\theta_1) - n^2}}{n^2 - 1} \qquad (3)$$

FIGURE 3. (a) MLB-MW unit structure diagram. (b) Simulation results of $|S_{21}|$ and $|S_{11}|$. (c) MLB-MW units equivalent circuit diagram: $R1 = R2 = 50\,\Omega$, $R3 - 8 = 25\,\Omega$, $L1 = L2 = 0.5\,\text{nH}$, $C1 = C2 = 4.3\,\text{pF}$, $L3 = L4 = L5 = 1.6\,\text{nH}$, $C3 = C4 = C5 = 1.3\,\text{pF}$.

The real part of r is always equal to 1, which means that MNG has perfect reflection properties. The reflection phase of MNG is: $\Phi_{MNG} = \tan^{-1}(\text{Im}(r))$. Both TE and TM polarizations lead to the same conclusion.

To enhance the antenna's bandwidth, we consider generating additional resonances with the MNG. At a specific frequency (f), the phase of the reflected wave at the antenna (Φ_r) can be expressed as:

$$\Phi_r = \Phi_{MNG} + 2\Phi_d \quad (4)$$

where Φ_d is the phase caused by the propagation path. Resonances occur when $\Phi_r = 2\pi m$ ($m = 0, 1, 2, \ldots$). We can derive that the distance between the antenna and MNG needs to satisfy the following condition:

$$d = \left(m + \frac{\theta_{MNG}}{2\pi}\right)\frac{c}{2f} \quad (m = 0, 1, 2, \ldots) \quad (5)$$

In this case, the constructive interference between the reflected wave and direct radiated wave enhances the electromagnetic field at the resonance position, thereby inducing additional current on the antenna surface. The enhancement of the surface current can improve the input impedance matching, thus increasing the bandwidth. In summary, the design process of the proposed antenna is as follows:

(1) Design an MNG decoupling wall with one or more stopbands, where the stopbands correspond to the operating frequency band of the antenna.

(2) Determine the resonant positions of the MNG that satisfy Equation (5).

(3) Place the antenna at the resonant position on each side of the MNG.

3. PERFORMANCE ANALYSIS OF MIMO ANTENNAS

The unit comprises a 1.6 mm thick single-layer FR-4 substrate ($\epsilon_r = 4.4$, $\tan\delta = 0.02$) and a metal wire substrate MNG. Figure 3(a) illustrates the design process of the proposed MLB-MW structure. By integrating two "middle" shaped patches into a closed loop, a notch-band resonance is generated at 10.6 GHz. As shown in Figure 3(b), the effective permeability in the desired frequency range is negative, indicating the characteristics of the MNG. This suppresses the propagation of electromagnetic waves. As illustrated in Figure 3(b), the MLB-MW exhibits clear band-stop characteristics ($|S_{21}|$) around 10.6 GHz. When being placed between the two antenna units, it effectively creates a high-isolation "electromagnetic tunnel" between them, preventing the direct coupling of surface waves and spatial waves. The structural parameters have been calculated and are provided in Figure 3(c). The substrate material selected is the widely available and cost-effective FR-4, with a thickness of 1.6 mm, which provides good mechanical strength and an optimal profile for microstrip antenna design. Although its loss tangent is slightly higher than that of high-frequency dedicated substrates, considering the manufacturing cost, processing convenience, and performance in the C to Ku band, FR-4 remains the best choice for this design, balancing both performance and cost.

When the distance (d) between the Floquet port and MLB-MW unit cell is 15 mm, the reflection phase is almost zero at 10 GHz. Due to the very thin substrate, the reflection characteristics of the MLB-MW are nearly identical on both sides. The equivalent circuit model of the MLB-MW is shown in Figure 3(c). The metal lines can be modeled as a series of LC resonators with a transmission zero, and the substrate layer can be modeled as a transmission line with an equivalent impedance

45

of 1 Z. The key structural dimensions of the metamaterial wall unit and individual antenna (such as $L1$-$L4$, $W1$-$W5$ in Figure 3(c), and La, Wa in Figure 5(a)) were determined through a systematic parametric analysis. This process primarily utilized the electromagnetic simulation software HFSS, with the optimization objectives of achieving the target bandwidth ($|S_{11}| < -10\,dB$) and high isolation ($||S_{21}| < -15\,dB$). The physical dimensions affecting resonance frequency and coupling strength were carefully adjusted: for instance, the metal line lengths of the MLB-MW ($L1$, $L2$, etc.) directly govern the series LC resonance frequency; the stepped patch dimensions of the single antenna (La, Lb, etc.) and the floor cut angle (Wg) were used to control current paths for impedance matching across the bandwidth. The final values of all geometric parameters are the results of this automated optimization iteration process, ensuring that the antenna's overall performance is maximized. The final geometric parameters are: $L1 = 16\,mm$, $L2 = 14\,mm$, $L3 = 10\,mm$, $L4 = 7\,mm$, $W1 = 10\,mm$, $W1 = 10\,mm$, $W2 = 8\,mm$, $W3 = 5\,mm$, $W4 = 7\,mm$, $W5 = 1\,mm$.

Figure 5(a) shows the topology of the proposed ultra-wideband omnidirectional antenna. The substrate material is FR-4 ($\epsilon_r = 4.4$, $\tan\delta = 0.02$), with a thickness of 1.6 mm. The $|S_{11}|$ is shown in Figure 5(b). By setting a stepped structure on the patch of the microstrip antenna, the antenna bandwidth is broadened, achieving ultra-wideband characteristics. The final geometric parameters are: $La = 16\,mm$, $Lb = 8\,mm$, $Lc = 2.8\,mm$, $Le = 1.6\,mm$, $Lg = 2.4\,mm$, $Wa = 20\,mm$, $Wb = 6\,mm$, $Wc = 1\,mm$, $Wh = 5.5\,mm$, $Wg = 7.9\,mm$, $Wf = 2.05\,mm$, $Wd = 3.9\,mm$, $We = 1.4\,mm$, $Lf = 4.03\,mm$.

To ensure that the antenna is in resonance, the distance between the two antennas (dx) is 13.6 mm, and the MLB-MW is placed in the center. Therefore, the vertical distance from the branch to the MLB-MW equals 6 mm.

In order to generate notches for WLAN, a U-shaped groove and a symmetric L-shaped groove are added to the third-order stepped rectangular radiating patch. As illustrated in Figure 4, an equivalent circuit of the dual-notch ultra-wideband antenna can be observed.
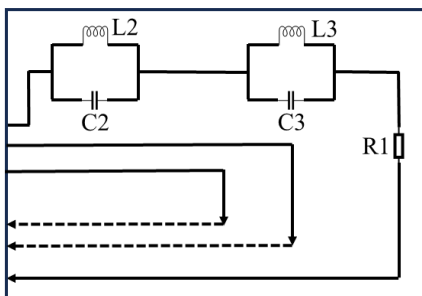

FIGURE 4. Trap wave equivalent circuit.

The length of the groove can be estimated using the following formula [20]:

$$L = \frac{c}{2f_0\sqrt{\epsilon_{eff}}}, \qquad \epsilon_{eff} = \frac{\epsilon_r + 1}{2} \qquad (6)$$

The formula is as follows: (L) represents the length of the groove; (c) denotes the speed of light; (f_0) is the center frequency corresponding to the stopband; (ϵ_r) and (ϵ_{eff}) are the relative permittivity and effective permittivity of the dielectric substrate, respectively. Based on Equation (6), when the center frequency is 10 GHz, the lengths of the inverted U-shaped groove and the symmetric L-shaped groove are approximately 3.6 mm and 4.7 mm, respectively. Through optimization using the electromagnetic simulation software HFSS, the optimal stopband characteristics are achieved when lengths of the inverted U-shaped groove and thesymmetric L-shaped groove are 3.9 mm and 4.9 mm, respectively, which adequately cover the WLAN frequency range.
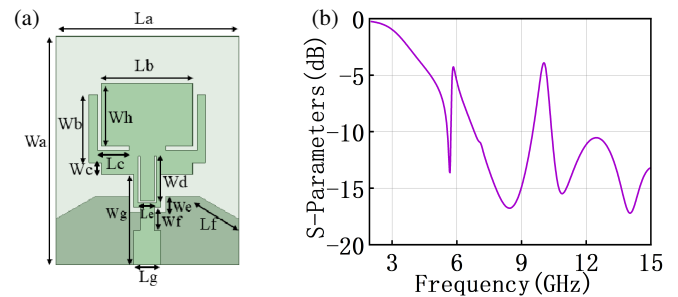

FIGURE 5. (a) The topology of the ultra-wideband microstrip antenna. (b) Reflection coefficient ($|S_{11}|$).

As shown in Figure 5(a), the dimensions of the antenna's dielectric substrate (approximately 16 mm × 20 mm) are derived using the classical formula based on the center frequency of the operating band. To ensure optimal antenna performance, adequate space must be reserved around the edges of the patch. It is generally recommended, based on experience, that the distance between the patch edge and the substrate boundary should be several times of the substrate thickness (in this design, a margin of approximately 2–4 mm is reserved on all sides) to avoid edge effects and effectively constrain the near-field radiation region. The characteristics of the antenna, including $|S_{11}|$ and $|S_{21}|$, are shown in Figure 6. Compared to the antenna without MLB-MW, the maximum mutual coupling is reduced by 10 dB, and $|S_{21}|$ is consistently below $-15\,dB$ across the frequency band. Meanwhile, the bandwidth ($|S_{11}| < -10\,dB$) is expanded from 6.09–13.07 GHz to 5.51–15 GHz, achieving a bandwidth extension rate of 35%. In the low-frequency range, the MLB-MW
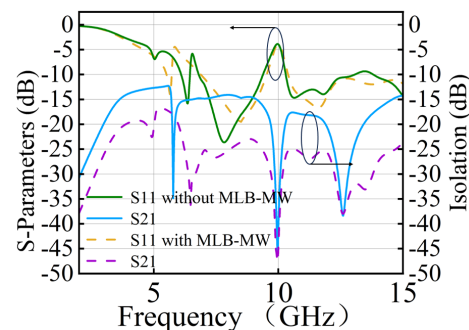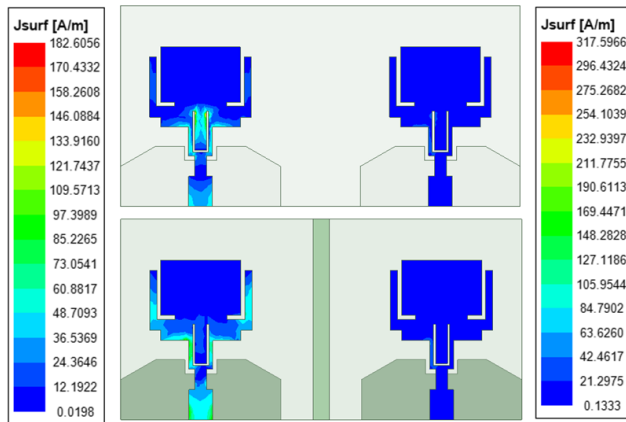

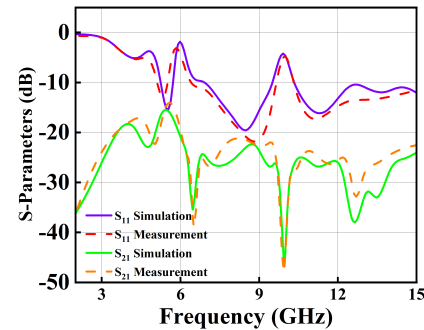FIGURE 6. Simulation results for the S-parameters of the proposed antenna.

FIGURE 7. Current distribution with or without MLB-MW at 11 GHz.

FIGURE 8. The S-parameters of the antenna from simulation and measurement.

structure introduces additional capacitive coupling, effectively compensating the inductive mismatch of the original antenna in this band. In the high-frequency range, the metallic line structure of MLB-MW creates new resonant modes, thereby shifting the antenna's high-frequency cutoff from 13.07 GHz to 15 GHz. While the bandwidth is extended, the notch characteristics (around 10 GHz) induced by the U-shaped and L-shaped slots on the radiation patch remain stable. This indicates that the introduction of MLB-MW primarily affects the antenna's fundamental mode and resonant characteristics, without significantly altering the current paths responsible for the notch, thus demonstrating the good independence between the two designs (notch and ultra-wideband). The surface current distribution in Figure 7 provides direct evidence for this. When MLB-MW is not loaded and Ant. 1 excited, a strong coupling current is observed on Ant. 2. However, after loading the MLB-MW, the current is effectively confined to the side of the excited antenna (Ant. 1), and the MLB-MW structure itself exhibits a high current concentration, indicating that it absorbs and dissipates the coupled energy. As a result, the current on the non-excited antenna (Ant. 2) is significantly reduced. This is the direct cause of the 10 dB improvement in isolation.

4. MEASUREMENT AND DISCUSSIONS

The prototype was manufactured and measured, as shown in Figures 11 and 12. The overall size of the antenna is 40 mm × 20 mm × 17.6 mm. Figure 8 presents the measured S-parameters. The measured bandwidth is 5.91–15 GHz. The error introduced by soldering affects the input impedance, causing slight reductions in the frequency bands and deterioration of the impedance matching. Compared to the case without MLB-MW, the measured isolation is still improved. However, due to soldering defects between the SMA connector and feed line, the measured results are generally lower than the simulations. In the measurements, by setting MLB-MW, both the bandwidth and isolation of the antenna were significantly improved, validating the effectiveness of the design method.

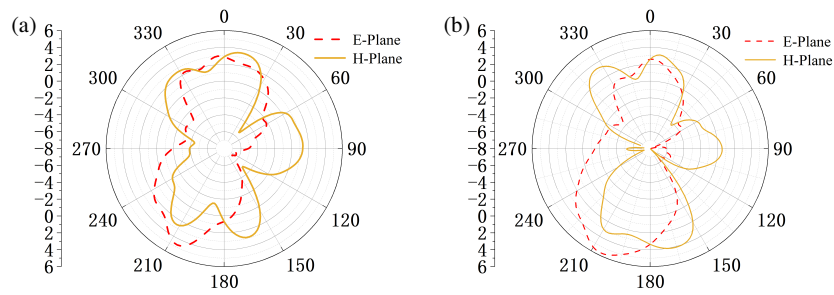The measured radiation pattern at 11 GHz is shown in Figure 9.

The diversity metrics of MIMO antennas, such as Envelope Correlation Coefficient (ECC), Diversity Gain (DG), and Total Active Reflection Coefficient (TARC), are shown in Figures 10(a), (b), and (c), respectively. In a MIMO configuration, the correlation between different antenna components is quantified by ECC. Lower ECC values indicate reduced interdependence between components, thereby enhancing the diversity performance of MIMO systems. Throughout the operating frequency range, the DG value ranges between 9.9 and 10, as shown in Figure 10(b). This value is used to evaluate the improvement in the signal-to-noise ratio brought about by diversity mechanism. It is evident that there is a positive correlation between ECC and DG parameters. Higher DG values signify better performance.

Compared to traditional reflection coefficients, TARC is crucial for determining the impedance bandwidth. The term TARC refers to the ratio of the square root of the total reflected power to the total incident power. This parameter is used to describe random signal combinations and mutual coupling between ports in a MIMO system. What makes TARC unique among MIMO parameters is that it takes into account the unpredictable phases of incident signals, which, in some cases, can significantly affect the behavior of the MIMO array.
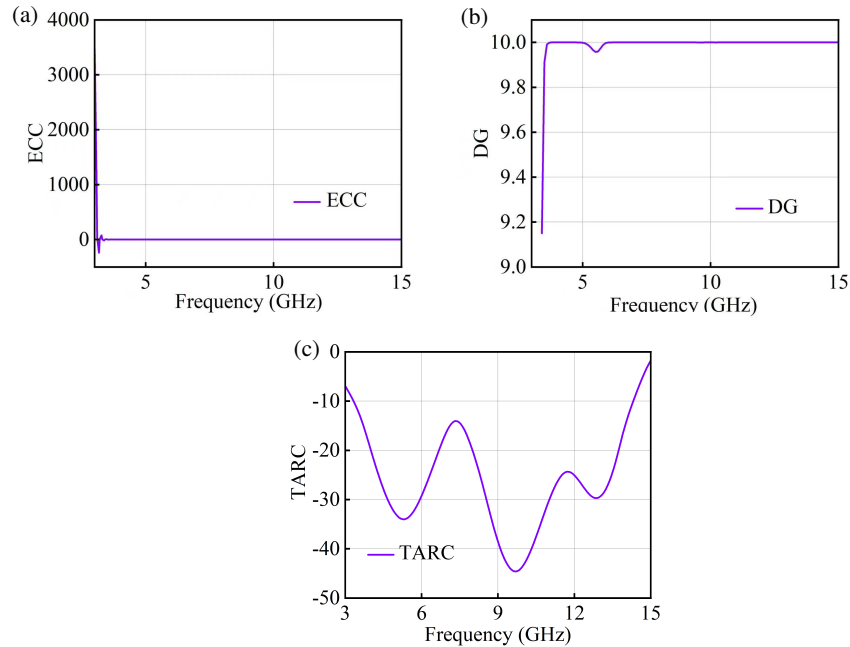
Table 1 provides a comparison of similar decoupling techniques. Compared to [2] and [11], this antenna offers a wider bandwidth and higher isolation. The disadvantage of this design is the introduction of some additional height. However, it is suggested that the MLB-MW not only improves antenna isolation but also enhances the bandwidth by up to 35%.
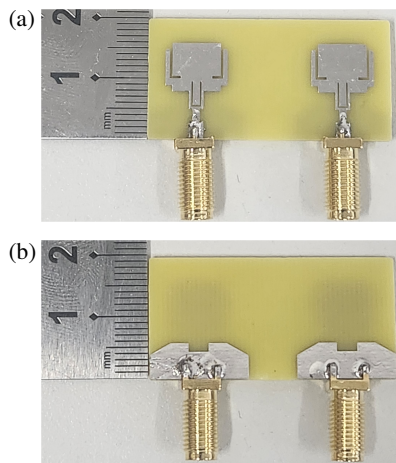
TABLE 1. Literature Comparison.

Ref.	Working Band	Isolation	Bandwidth Improvement
[2]	3.3–5 GHz	21 dB	lack
[5]	3–10 GHz	38 dB	lack
[11]	2–14 GHz	20 dB	lack
[14]	3.2–8.4 GHz	20 dB	lack
[15]	3.1–10.6 GHz	18 dB	lack
This work	5.51–15 GHz	25 dB	35%

FIGURE 9. (a) The measured radiation pattern at 11 GHz without MLBMW. (b) The measured radiation pattern at 11 GHz with MLB-MW.
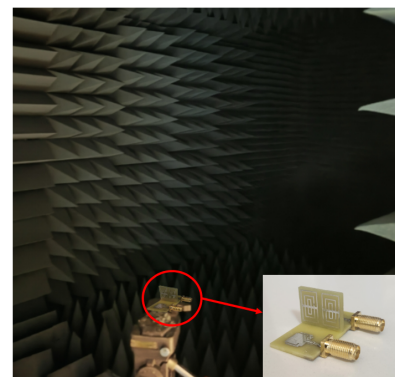

FIGURE 10. MIMO diversity parameters. (a) ECC. (b) DG. (c) TARC.

FIGURE 11. (a) Top view of the physical object. (b) Back view of the physical object.

FIGURE 12. Current distribution with or without MLB-MW at 11 GHz.

5. CONCLUSION

A new method is proposed to improve MIMO antenna isolation and bandwidth using metamaterial (MM) walls. The proposed MLB-MW has two band-stop resonance frequencies at 8 GHz and 13.6 GHz. By placing a microstrip antenna at the resonance positions, a 35% bandwidth extension is achieved. At the same time, the isolation is improved by 10 dB. This antenna has advantages such as a simple structure, ease of design, and low cost, making it suitable for application in 5G base stations. This study demonstrates a fixed-notch functionality. A key direc-

tion for future work is the incorporation of tunable components, such as PIN diodes or varactors, to enable dynamic electronic control of the notch frequency and operating band. This would pave the way for developing reconfigurable UWB-MIMO antennas capable of intelligently adapting to complex electromagnetic environments.

REFERENCES

[1] Potti, D., Y. Tusharika, M. G. N. Alsath, S. Kirubaveni, M. Kanagasabai, R. Sankararajan, S. Narendhiran, and P. B. Bhargav, "A novel optically transparent UWB antenna for automotive MIMO communications," *IEEE Transactions on Antennas and Propagation*, Vol. 69, No. 7, 3821–3828, 2021.

[2] Sun, L., Y. Li, Z. Zhang, and Z. Feng, "Wideband 5G MIMO antenna with integrated orthogonal-mode dual-antenna pairs for metal-rimmed smartphones," *IEEE Transactions on Antennas and Propagation*, Vol. 68, No. 4, 2494–2503, 2020.

[3] Kong, Q., P. Zhang, L. Chen, and J. Bai, "High-isolation compact wideband MIMO antennas for 5G smartphones with unbroken metal frames," *Electronics*, Vol. 14, No. 19, 3852, 2025.

[4] Dutta, D., P. Ghosh, and A. Gorai, "A wideband millimeter-wave MIMO antenna for 5G applications in the n260 frequency band," *2023 IEEE Silchar Subsection Conference (SILCON)*, 1–4, Nov. 2023.

[5] Nie, L. Y., X. Q. Lin, Z. Q. Yang, J. Zhang, and B. Wang, "Structure-shared planar UWB MIMO antenna with high isolation for mobile platform," *IEEE Transactions on Antennas and Propagation*, Vol. 67, No. 4, 2735–2738, 2019.

[6] Gómez-Villanueva, R. and H. Jardón-Aguilar, "Compact UWB uniplanar four-port MIMO antenna array with rejecting band," *IEEE Antennas and Wireless Propagation Letters*, Vol. 18, No. 12, 2543–2547, 2019.

[7] Wang, L., Z. Du, H. Yang, R. Ma, Y. Zhao, X. Cui, and X. Xi, "Compact UWB MIMO antenna with high isolation using fence-type decoupling structure," *IEEE Antennas and Wireless Propagation Letters*, Vol. 18, No. 8, 1641–1645, 2019.

[8] Li, Z., C. Yin, and X. Zhu, "Compact UWB MIMO Vivaldi antenna with dual band-notched characteristics," *IEEE Access*, Vol. 7, 38 696–38 701, 2019.

[9] Khandekar, R. and D. Sipal, "Design and analysis of mm-Wave MIMO antenna with a UWB AMC," *IEEE Antennas and Wireless Propagation Letters*, Vol. 24, No. 9, 2944–2948, 2025.

[10] Zhao, X., S. Riaz, and S. Geng, "A reconfigurable MIMO/UWB MIMO antenna for cognitive radio applications," *IEEE Access*, Vol. 7, 46 739–46 747, 2019.

[11] Jayant, S., G. Srivastava, and S. Kumar, "Quad-port UWB MIMO footwear antenna for wearable applications," *IEEE Transactions on Antennas and Propagation*, Vol. 70, No. 9, 7905–7913, 2022.

[12] Yang, Y., Q. Chu, and C. Mao, "Multiband MIMO antenna for GSM, DCS. and LTE indoor applications," *IEEE Antennas and Wireless Propagation Letters*, Vol. 15, 1573–1576, 2016.

[13] Li, W., L. Wu, S. Li, X. Cao, and B. Yang, "Bandwidth enhancement and isolation improvement in compact UWB-MIMO antenna assisted by characteristic mode analysis," *IEEE Access*, Vol. 12, 17 152–17 163, 2024.

[14] Wu, L., Y. Xia, X. Cao, and Z. Xu, "A miniaturized UWB-MIMO antenna with quadruple band-notched characteristics," *International Journal of Microwave and Wireless Technologies*, Vol. 10, No. 8, 948–955, 2018.

[15] Premalatha, B., G. Srikanth, and G. Abhilash, "Design and analysis of multi band notched MIMO antenna for portable UWB applications," *Wireless Personal Communications*, Vol. 118, 1697–1708, 2021.

[16] Desai, A., J. Kulkarni, M. M. Kamruzzaman, Š. Hubálovský, H.-T. Hsu, and A. A. Ibrahim, "Interconnected CPW fed flexible 4-port MIMO antenna for UWB, X, and Ku band applications," *IEEE Access*, Vol. 10, 57 641–57 654, 2022.

[17] Zhao, L., Y. Wang, C. Liu, D. Song, C. Hu, C. Li, H. Zhao, and Z. Wang, "Compact circular-shaped MIMO antenna covers UWB bandwidth with four frequently-used band-notched characteristics for multi-scenario applications," *IEEE Access*, Vol. 12, 32 762–32 771, 2024.

[18] Rekha, V. S. D., P. Pardhasaradhi, B. T. P. Madhav, and Y. U. Devi, "Dual band notched orthogonal 4-element MIMO antenna with isolation for UWB applications," *IEEE Access*, Vol. 8, 145 871–145 880, 2020.

[19] Wang, H., Q. Zheng, Q. Li, and X.-X. Yang, "Isolation improvement and bandwidth enhancement of dual-band MIMO antenna based on metamaterial wall," *IEEE Antennas and Wireless Propagation Letters*, Vol. 24, No. 5, 1144–1148, 2025.

[20] Zhang, Y., F.-S. Zhang, R. Zou, Y.-B. Yang, and F. Ding, "Design of an novel ultra-wideband antenna with dual band-notched characteristics," *Proceedings of 2011 IEEE CIE International Conference on Radar*, 1179–1181, 2011.